Plant, Cell & Environment

Plant, Cell and Environment (2013) **36**, 1755–1770 doi: 10.1111/pce.12115

Closing in on maximum yield of chlorophyll fluorescence using a single multiphase flash of sub-saturating intensity

S. D. LORIAUX[1], T. J. AVENSON[1], J. M. WELLES[1], D. K. MCDERMITT[1], R. D. ECKLES[1], B. RIENSCHE[1] & B. GENTY[2,3,4]

[1]LI-COR Biosciences, 4647 Superior Street, Lincoln, NE, USA, [2]CEA, DSV, IBEB, Laboratoire d'Ecophysiologie Moléculaire des Plantes, 13108 Saint-Paul-lez-Durance, France, [3]CNRS, UMR 7265 Biologie Végétale et Microbiologie Environnementales, 13108 Saint-Paul-lez-Durance, France and [4]Université Aix-Marseille, 13108 Saint-Paul-lez-Durance, France

ABSTRACT

Estimation of the maximum chlorophyll fluorescence yield under illumination, or Fm′, by traditional single saturation pulse (SP) methodology is prone to underestimation error because of rapid turnover within photosystem (PS) II. However, measurements of fluorescence yield during several single pulses of variable intensity describes the irradiance dependence of apparent Fm′, from which estimates of Fm′ at infinite irradiance can be derived. While such estimates have been shown to result in valid approximations of Fm′, the need to apply several single pulses limits its applicability. We introduce a novel approach that determines the relationship between apparent Fm′ and variable irradiance within a single ~1 s multiphase flash (MPF). Through experiments and simulations, we demonstrate that the rate of variation in irradiance during an MPF is critical for achieving quasi–steady-state changes in the proportions of PSII acceptor side redox intermediates and the corresponding fluorescence yields, which are prerequisites for accurately estimating Fm′ at infinite irradiance. The MPF methodology is discussed in the context of improving the accuracy of various parameters derived from chlorophyll fluorescence measurements, such as photochemical and non-photochemical quenchings and efficiencies. The importance of using MPF methodology for interpreting chlorophyll fluorescence, in particular for integrating fluorescence and gas exchange measurements, is emphasized.

Key-words: CO_2 assimilation; efficiency; electron transport; leaf gas exchange; mesophyll conductance; non-photochemical quenching; photochemistry; quantum yield; saturating pulse.

INTRODUCTION

The wide use of chlorophyll fluorescence to understand many biophysical and physiological aspects of photosynthesis in intact photosynthetic organisms over recent decades has been largely driven by advances in both instrumentation and methodology. Thanks to progress in optoelectronics [e.g. light-emitting diodes (LEDs) as pulsed measuring light sources], as well as miniaturized electronics for signal detection and processing, chlorophyll fluorescence elicited by pulsed dim light of constant intensity can be readily used to probe the relative change in fluorescence yield (ΦF) while minimizing actinic effects of the measuring light on photosynthesis (Ogren & Baker 1985; Schreiber, Schliwa & Bilger 1986). This methodology is generically termed modulated or pulse–amplitude-modulated (PAM) fluorometry and allows monitoring of the relative change in ΦF under actinic illumination.

Combination of the saturation light pulse approach (Bradbury & Baker 1981; Dietz, Schreiber & Heber 1985; Ogren & Baker 1985; Schreiber *et al*. 1986) with PAM methodology allows straightforward estimates of characteristic states of maximum ΦF, which are commonly referred to as Fm or Fm′ when measured under darkness or actinic illumination, respectively (van Kooten & Snel 1990). The saturating pulses (SP) of light typically used to measure Fm′ involve rapid and transient increases in photosynthetic photon flux density (PPFD) to maxima that are several-fold higher than full sunlight irradiance and are held constant for ~0.5–1 s (Ogren & Baker 1985; Schreiber *et al*. 1986; Schreiber 2004). According to the dynamics of photosystem (PS) II photochemistry and PSII acceptor reactions, the intensity and duration of a SP are intended to cause the transient, complete reduction of both the primary quinone acceptor in PSII (Q_A) and the plastoquinone (PQ) pool, both of which are necessary for accurate determination of Fm′. However, complete reduction of Q_A may be hindered by rapid turnover of the PSII acceptor pools, even when using very high SP intensities (Markgraf & Berry 1990).

The potential for underestimation of Fm′ is important considering how widely it, and many parameters derived from it, are used in many analytical fields requiring precise, quantitative measurements. Estimates of Fm′ are used in conjunction with other characteristic fluorescence states to calculate insightful parameters that relate to photochemical and non-photochemical quenching processes at PSII, as well as their efficiencies (e.g. qP, qN, NPQ). Of particular relevance for physiological studies are estimates of the quantum efficiency of PSII-mediated electron transport, or Φ_{PSII} [$\Phi_{PSII} = (Fm' - F)/Fm'$] and the corresponding flux of electrons through PSII (J) (Genty, Briantais & Baker 1989). These estimates not only provide a quantification of the rate of photochemistry using simple optical measurements, but they also provide an insightful tool to describe the processes involved in photosynthesis when used in combination with other methods (e.g. gas analysis, absorption spectroscopy). For example, the number of electrons required to assimilate CO_2 can be obtained from a comparison of J and gross CO_2 assimilation (A_G) (Krall & Edwards 1990; Laisk & Loreto

Correspondence: B. Genty. Tel: +33 442254397; e-mail: bernard.genty@cea.fr

© 2013 John Wiley & Sons Ltd

1996). Estimation of J is important for assessing electron flow to alternate electron sinks in the chloroplast (Ruuska *et al.* 2000) and the relative rates of linear versus cyclic electron transport (Harbinson & Foyer 1991; Avenson *et al.* 2005). Simultaneous measurements of J and CO_2 assimilation can be used to estimate the CO_2 concentration at the site of carboxylation (C_c), from which mesophyll conductance to CO_2 (g_m) can be determined (Harley *et al.* 1992; Pons *et al.* 2009).

More accurate estimates of true Fm′, which compensate for underestimation due to acceptor turnover, can be obtained from the dependence of ΦF on irradiance. ΦF increases hyperbolically towards an asymptote as SP irradiance (Q′) increases (Markgraf & Berry 1990). Markgraf and Berry (1990) and Earl and Ennahli (2004) showed that ΦF was linearly related with $(Q')^{-1}$, the reciprocal of Q′, at high irradiance. Linear regression and extrapolation of ΦF to $(Q')^{-1} = 0$ provided estimates of Fm′ at infinite irradiance that were consistently higher than those measured at the highest irradiance. The authors used a series of distinct SP's of varying intensity to obtain the dependence of Fm′ on irradiance. Obtaining an extrapolated estimate of Fm′ using this approach requires a series of variably intense Q′, each separated by several minutes, which significantly limits experimental throughput.

In this paper, we describe a novel saturation-pulse method referred to as a multiphase flash (MPF) that is capable of rapidly (i.e. within less than 1 s) describing the irradiance dependency of Fm′ and estimating Fm′ at infinite irradiance. For this purpose, a variation of irradiance is included within the duration of the flash which involves three irradiance regimes: 'phase' 1 where a constant maximum irradiance is achieved, phase 2 where irradiance is attenuated (i.e. 'ramped'), and phase 3 where the irradiance is set to the initial maximum phase 1 level. Comprehensive modeling and empirical approaches are used to demonstrate the accuracy and applicability of the MPF-derived estimates of Fm′. The importance of using accurate fluorescence parameters derived from the MPF method, in particular for integrating fluorescence and gas exchange measurements, is discussed. A preliminary report of some of this work was presented earlier (Loriaux *et al.* 2006).

MATERIALS AND METHODS

Plant material

Leaves of field grown plants of sunflower (*Helianthus annuus*) and maize (*Zea mays*) were used to characterize MPF dynamics and to demonstrate the applicability of the MPF method during combined fluorescence and gas exchange measurements in the field. Plants were grown at the University of Nebraska (Summer 2006) and in an experimental garden (Spring and Summer 2008 and 2010) at LI-COR Inc. (Lincoln, NE, USA). When fluorescence measurements were performed in the laboratory, leaves were cut at their petiole and the cut portions of the stems were immediately placed in water in order to maintain the leaf in a hydrated state. The portion of the leaf being analysed was clamped into the measuring chamber (see later) and exposed to actinic light in order to achieve steady photosynthetic activity as assessed by fluorescence and gas exchange, if measured simultaneously.

Fluorometer for MPF characterization

A lab-based chlorophyll fluorometer for simultaneously measuring continuous and pulse-modulated fluorescence was developed for the experiments described herein. The sampled leaf area was defined by a one inch diameter aperture and measurements were performed in a dark room. Actinic light, including flashes, was provided by two identical red LED arrays (Lighting Science Group, NT-51A0-0468, Satellite Beach, FL, USA) spaced 1.5 inches away from the leaf and positioned slightly off axis from normal to the leaf. The LED arrays had a peak emission wavelength of 635 nm and a half-peak bandwidth of 20 nm. The emitters were filtered with a short-pass optical filter with a cut off wavelength of 700 nm (Edmund Optics, 54516, Barrington, NJ, USA). Light output, up to 15 000 μmol m^{-2} s^{-1} irradiance, was regulated by optical feedback from an unfiltered photodiode (Advanced Photonix Inc., PDB-C170, Ann Arbor, MI, USA). The settling time of the regulation of the LED light output had a 2 μs time constant. Measuring pulsed light was provided by a single LED (model LSE6SF, Osram, Munich, Germany) with peak emission of 645 nm and a half band width of 16 nm. Optical filtering was done with a 650 nm short-pass filter (Andover Corp 650FL07, Salem, NH, USA). Pulse widths were 2 μs and had rise and fall times of less than 100 ns. Measuring intensity was selectable to 0.0001 μmol m^{-2} per pulse and rates could be set from 0.2 to 200 kHz. Fluorescence emitted from the leaf was focused with a lens (AC080-010-B, Thorlabs, Newton, NJ, USA) onto a silicon PIN photodiode (S1223-01, Hamamatsu, Hamamatsu City, Japan). The fluorescence detector was mounted with two filters in series: a long-pass absorption filter with a 715-nm cut-off (FGL715, Thorlabs) and a long-pass interference filter with a cut-off of 700 nm (700FH90-50S, Andover Corporation). The fluorescence detector signal was amplified with a low-noise transimpedance amplifier, and was AC coupled to another amplifier with a gain of 100×. The continuous fluorescence was measured directly from the transimpedance amplifier. The modulated fluorescence was detected from the 100× amplified signal with sample and hold amplifiers that were phase aligned with the measuring LED modulation. The signals were filtered with a 200 Hz second-order Bessel low-pass filter. National Instruments (Austin, TX, USA) data acquisition card (NI 6251) and LabVIEW software (National Instruments) were used to control and acquire signals from the fluorometer apparatus.

For achieving the best signal-to-noise ratio, MPF characterization was carried out using the continuous fluorescence signal. Relative fluorescence yield was derived from the continuous fluorescence signal as the ratio of the continuous fluorescence signal divided by the continuous actinic irradiance signal monitored by the photodiode used for optical feedback regulation. It should be noted that the continuous and modulated signals did not give significantly different results (data not shown).

Combined fluorescence and gas exchange

Simultaneous fluorescence, including that based on MPF methodology, and gas exchange measurements were collected using LI-6400 Portable Photosynthesis Systems with 6400-40 Leaf Chamber Fluorometers (LI-COR Inc., Lincoln, NE, USA). The leaf chamber conditions were controlled in order to maintain ambient CO_2 concentrations of 370–380 μmol mol^{-1}, average leaf temperatures of 30.3°C ($\pm$0.16), and average vapour pressure deficits of 1.94 ($\pm$0.04) kPa. The fluorometer settings for flashes including both traditional rectangular flashes (RFs) and MPF's were: modulation rate of 20 kHz, 50 Hz averaging filter, and measuring intensity of 0.0002 μmol m^{-2} pulse^{-1}.

J was calculated as the product of $\Phi_{PSII} = (Fm' - F)/Fm'$, where F is the steady fluorescence level, the fraction of incident light partitioned to PSII (f_{II}), incident light intensity (i), and leaf absorbance (α) (i.e. $J = \Phi_{PSII} \cdot f_{II} \cdot i \cdot \alpha$). The value of f_{II} was assumed to be 0.5 and i was measured with an internal PAR sensor. Estimates of α were calculated as: $\alpha = [\alpha_{blue} \cdot B + \alpha_{red} \cdot (100 - B)]/100$ where B is the percentage of i that is blue, and α_{blue} and α_{red} are the respective blue and red LED absorptance values measured using a spectroradiometer and integrating sphere (LI-1800, LI-COR Inc.) for each species. Values of α_{blue} and α_{red} for maize and sunflower were 0.91 and 0.85 and 0.89 and 0.87, respectively. g_m was estimated by the variable J method (Harley *et al*. 1992).

Modelling and simulations

For simulating the dynamics of fluorescence during an MPF, a mechanistic model was developed that was largely inspired from those previously designed for simulating fluorescence induction under constant irradiance regimes in the absence of acceptor-side inhibition (Renger & Schulze 1985; Baake & Schloder 1992; Stirbet *et al*. 1998; Lazar 2003; Zhu *et al*. 2005; Kroon & Thoms 2006). The model describes the irradiance-dependency of the fate of excitation in PSII in relation to the rates of PSII photochemistry and of the electron-transport reactions on the acceptor side of PSII. In order to simulate the variations of ΦF, which minimizes complexity, the modelling framework only considered the PSII-acceptor side and ignored the donor-side reactions. This seems justified because for the light regime and the time domain used during phase 2 of an MPF, (slow change of irradiance relative to the initial irradiance, approx. 0.2% per ms, and several tens of ms time interval for the ramp phase, respectively), the effects of the donor-side and related reactions (i.e. the S-states) are predicted to be small. Thus, in these conditions, oxidized P680 ($P680^+$), a strong quenching species, does not significantly contribute to the variations of ΦF.

The model integrates components of both PSII photochemistry and electron transfer on the acceptor-side of PSII. The *photochemical component* describes the reactions that generate charge separation (i.e. radical pair formation) and stabilization (i.e. reduction of Q_A) within PSII. The relationships between the redox state of Q_A, and the fluorescence and photochemical yields were derived according to the approach proposed by Lavergne & Trissl (1995). This model considers two important features of PSII photophysics: the reversibility of the primary charge separation (exciton radical-pair equilibrium model) and restricted exciton transfer between PSII units (i.e. finite connectivity), where unit refers to an antenna and associated reaction centre. The PSII *acceptor-side component* describes the electron transport reactions from Q_A^- to Q_B (i.e. the secondary electron acceptor in the PSII reaction centre) the PQ pool, and the cytochrome b_6f complex in the framework of the so-called 'two-electron gate' model (Renger & Schulze 1985; Baake & Schloder 1992; Stirbet *et al*. 1998; Zhu *et al*. 2005). The rate equations representing these reactions were derived under the assumptions that all PSII complexes consist of Q_B-reducing reaction centres and that the PQ pool is homogenously involved in electron transport. To limit the set of reactions, the model did not explicitly include the reactions of Q_B-binding to its site at the D1 protein, as was implemented in the model of Kroon & Thoms (2006). After merging the photochemical and acceptor-side components, the resulting integrated model is formally similar to that of Baake & Schloder (1992), except that non-photochemical quenching by PQ was also included, as described in Lazar (2003) and Zhu *et al*. (2005).

The photochemical component

The model considers the bulk of PSII's as a 'bed' of interconnected PSII units with open and closed reaction centres, depending on whether the primary quinone acceptor is oxidized (Q_A) or reduced (Q_A^-), respectively (Fig. 1). Because exciton transfer within each unit is assumed to be fast in comparison with charge separation, the exciton density within the bed was considered uniform. The fate of the excitation within a given PSII unit (U) was described using a set of first-order rate constants, namely: K_p, for decay of an exciton through charge separation and subsequent charge

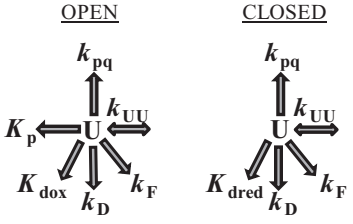

Figure 1. Photochemical reactions in PSII units with open and closed reaction centres. The fate of the excitation within a given PSII unit (U) was described using a set of first-order rate constants, namely: K_p, for decay of an exciton through charge separation and subsequent charge stabilization in an open centre (i.e. formation of Q_A^-); K_{dox} and K_{dred}, for decay through charge separation and subsequent non-radiative losses in open and a closed centres, respectively; k_D, for non radiative losses in the antenna that include losses involving photoprotective, non-photochemical quenching processes; k_{PQ}, for non-radiative losses dependent on non-photochemical quenching by plastoquinone (PQ); k_F, for radiative losses (fluorescence); and k_{UU} for inter-unit exciton transfer. The values of the rate constants can be found in Table 1.

stabilization in an open centre (i.e. formation of Q_A^-); K_{dox} and K_{dred}, for decay through charge separation and subsequent non-radiative losses in open and closed centres, respectively; k_D, for non-radiative losses in the antenna that include losses involving photoprotective, non-photochemical quenching (qN) processes; k_{PQ}, for non-radiative losses dependent on non-photochemical quenching by PQ; k_F, for radiative losses (i.e. fluorescence); and k_{UU} for inter-unit exciton transfer. Capitals are used for K_p, K_{dox} and K_{dred} to emphasize that these are *apparent* rate constants and represent ratios of rate constants for several steps that primarily involve reversible charge separation and charge stabilization or non-radiative losses. K_p, K_{dox} and K_{dred} are equivalent to α_p, α_d and β, respectively, as defined in Lavergne & Trissl (1995), and allow a more simplified description of exciton decay in the framework of the exciton-radical pair equilibrium model.

Within a given PSII unit, the fate of excitons can be described by probability, or yield, terms for various pathways. Fluorescence yields (ϕF) can be described as:

$$\phi Fred = \frac{kF}{kF + kD + Kdred + kpq \cdot p + kUU} \quad (1)$$

$$\phi Fox = \frac{kF}{kF + kD + Kdox + Kp + kpq \cdot p + kUU} \quad (2)$$

where $\phi Fred$ and ϕFox indicate yield for units with closed (i.e. reduced Q_A^-) and open (i.e. oxidized Q_A) reaction centres, respectively, and p represents the proportion of PQ (i.e. $[PQ]/([PQ] + [PQH_2])$).

The yields of inter-unit exciton transfer (ϕUU) can be similarly described as:

$$\phi UUred = \frac{kUU}{kF + kD + Kdred + kpq \cdot p + kUU} \quad (3)$$

$$\phi UUox = \frac{kUU}{kF + kD + Kdox + Kp + kpq \cdot p + kUU} \quad (4)$$

and the yield of PSII-mediated photochemistry (ϕp) as:

$$\phi p = \frac{Kp}{kF + kD + Kdox + Kp + kpq \cdot p + kUU} \quad (5)$$

Assuming a random walk migration of excitons between PSII units, the fate of exciton decay within the whole bed of PSII units via fluorescence, or the yield of fluorescence for the whole bed of PSII (ΦF), can be described by an infinite series as:

$$\Phi F = \phi F\left(1 + \phi UU + \phi UU^2 + \phi UU^3 + \ldots\right) \quad (6)$$

that can be simply expressed as:

$$\Phi F = \frac{\phi F}{1 - \phi UU} \quad (7)$$

where ϕF and ϕUU correspond to the yields of fluorescence and inter-unit exciton transfer, respectively, for the whole PSII bed according to:

$$\phi F = (1 - q) \cdot \phi Fred + q \cdot \phi Fox \quad (8)$$

$$\phi UU = (1 - q) \cdot \phi UUred + q \cdot \phi UUox \quad (9)$$

where q represents the proportion of open reaction centres (i.e. $[Q_A]/([Q_A] + [Q_A^-])$).

Then, according to a similar rationale as used to derive Eqns 6 and 7, the yield of photochemistry for the whole bed of PSII (Φp) can be derived as:

$$\Phi p = \frac{q \cdot \phi p}{1 - \phi UU} \quad (10)$$

The acceptor side component

The chemical species and the reactions at the acceptor side of PSII that were included in the model are shown in Fig. 2. All acceptor-side reactions were treated as being first-order, except the exchange of PQ between the Q_B site and the PQ/PQH_2 pool, a process that was treated as a second-order reaction (Zhu *et al.* 2005). According to the scheme, the redox state of the PSII acceptor-side can be described by six different redox states of Q_A and Q_B, each of which is labelled A. . .F. UQ_AQ_B, $UQ_AQ_B^-$, $UQ_AQ_B^{2-}$ represent units with open centres (A–C) and $UQ_A^-Q_B$, $UQ_A^-Q_B^-$, $UQ_A^-Q_B^{2-}$ represent units with closed centres (D–F).

Following the rationale of the previous section, mathematics were simplified by describing the concentrations of the various redox states of the reaction centre as proportions (i.e. relative variables). Therefore, the proportions of open (q) and closed ($1 - q$) PSII centres defined in the previous section can be expressed, respectively, as:

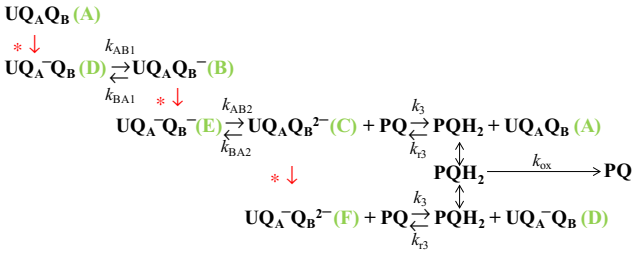

Figure 2. PSII acceptor-side reactions. This scheme describes the electron transport reactions from Q_A^- to Q_B, the PQ pool, and the cytochrome b_6f complex in the framework of the so-called 'two-electron gate' model. The model used to simulate multiphase flash (MPF) dynamics incorporated rate constants for the electron transfer reactions on the acceptor-side of PSII: k_{AB1}, describes electron transfer from $UQ_A^-Q_B$ to $UQ_AQ_B^-$; k_{BA1}, describes electron transfer from $UQ_AQ_B^-$ to $UQ_A^-Q_B$; k_{AB2}, describes electron transfer from $UQ_A^-Q_B^-$ to $UQ_AQ_B^{2-}$; k_{BA2}, describes electron transfer from $UQ_AQ_B^{2-}$ to $UQ_A^-Q_B^-$; k_3 describes electron transfer from $UQ_AQ_B^{2-}$ to PQH_2; k_{r3} describes electron transfer from PQH_2 to $UQ_AQ_B^{2-}$; and k_{ox} describes oxidation of PQH_2 at the cytochrome b_6f complex. The red arrow (plus asterisk) represents photochemical injection of an electron into the reaction centre. The values of the rate constants can be found in Table 2.

$$q = a + b + c \text{ and } (1 - q) = d + e + f \tag{11}$$

where a, b, c, d, e and f represent the proportions of centres in states A, B, C, D, E and F, respectively, and were calculated as [A]/([A] + [B] + [C] + [D] + [E] + [F]). . . . [F]/([A] + [B] + [C] + [D] + [E] + [F]), respectively, where quantities in brackets represent concentrations.

Following the approach developed to derive Eqn 10, it can be shown that the photochemical yield can be simply partitioned for each of the three different open states as:

$$\Phi p_i = \frac{x_i}{q} \cdot \Phi p \tag{12}$$

where Φp_i is the photochemical yield from centres in open state i and x_i is the fraction of centres in open state i (i.e. a, b or c).

The relative rate of photochemical reduction of Q_A in each open state, or ε_i, can then be calculated as:

$$\varepsilon_i = \frac{ia \cdot N}{([Q_A] + [Q_A^-])} \cdot \Phi p_i \tag{13}$$

where the first term corresponds to the relative rate of excitation at PSII in which ia and N are the absorbed photon flux density and the fraction of absorbed photons partitioned to PSII, respectively.

Finally, combination of both the photochemical and acceptor-side reactions leads to the following system of ordinary differential equations (ODE) that were used to describe the time dependencies of the chemical species involved in the time dependent change of ΦF:

$$\frac{d}{dt} a(t) = k3 \cdot p(t) \cdot c(t) - kr3 \cdot (1 - p(t)) \cdot a(t) - \varepsilon_a(t) \tag{14a}$$

$$\frac{d}{dt} d(t) = \varepsilon_a(t) - kAB1 \cdot d(t) + kBA1 \cdot b(t) + k3 \cdot p(t) \cdot f(t) - kr3 \cdot (1 - p(t)) \cdot d(t) \tag{14b}$$

$$\frac{d}{dt} b(t) = -\varepsilon_b(t) + kAB1 \cdot d(t) - kBA1 \cdot b(t) \tag{14c}$$

$$\frac{d}{dt} e(t) = \varepsilon_b(t) + kBA2 \cdot c(t) - kAB2 \cdot e(t) \tag{14d}$$

$$\frac{d}{dt} c(t) = -\varepsilon_c(t) - kBA2 \cdot c(t) + kAB2 \cdot e(t) - k3 \cdot p(t) \cdot c(t) + kr3 \cdot (1 - p(t)) \cdot a(t) \tag{14e}$$

$$\frac{d}{dt} f(t) = \varepsilon_c(t) - k3 \cdot p(t) \cdot f(t) + kr3 \cdot (1 - p(t)) \cdot d(t) \tag{14f}$$

$$\frac{d}{dt}(1 - p(t)) = \frac{k3 \cdot p(t) \cdot c(t)}{n} - \frac{kr3 \cdot (1 - p(t)) \cdot a(t)}{n} + \frac{k3 \cdot p(t) \cdot f(t)}{n} - \frac{kr3 \cdot (1 - p(t)) \cdot d(t)}{n} - kox \cdot (1 - p(t)) \tag{14g}$$

where the signification of the rate constants is given in Fig. 2 and n is the size of the PQ pool relative to total Q_A (i.e. $n = ([PQ] + [PQH_2])/([Q_A] + [Q_A^-])$. Recall that $q = a + b + c$ and note that the time dependent variables are a, b, c, d, e, f, p and ε_i. ε_i is calculated from the time dependency of ia using Eqn 13.

As such, another ODE is required to describe the time dependency of ia during the ramp phase of the MPF, which is:

$$\frac{d}{dt} ia(t) = -\theta \tag{15}$$

where θ is the ramp slope.

Solving rationale for MPF simulations

First, the system of ODE's (Eqn 14) was numerically solved for steady state at a given ia. This provides a corresponding set of redox states for PSII reaction centres and the PQ pool, for example $a \ldots f$ and p, respectively. This set is assumed to show the states describing what is tantamount to the end of phase 1 of a simulated MPF for this given constant ia and is used as the initial conditions for the subsequent solving step. Then, using these initial conditions, the system of ODE's was modified to include time dependent change of ia (i.e. combining Eqns 14a–14g and 15) and solved numerically for describing the ramp phase of MPF (phase 2). This provides the time dependency *of* ia, $a \ldots f$ and p during the simulated phase 2. Subsequently, the corresponding time dependency of ΦF was calculated using Eqn 7 and was used to analyse the change of ΦF versus the change of ia during phase 2.

Numerical solving was performed using Maple version 11 software (Maplesoft, Waterloo, ON, Canada). For solving the ODE system that is stiff, the numerical algorithm that was routinely used is based on an Implicit Rosenbrock third–fourth-order Runge-Kutta method. Use of a more accurate algorithm that invokes Gear's method in the Livermore Stiff ODE solver of Maple did not significantly change the simulation results.

For simulations, the values of input parameters, which are rate constants, initial concentrations and relative stoichiometries, are given in Tables 1, 2 and 3. The values are similar to those reported in previous studies (Lavergne & Trissl 1995; Lazar 2003; Zhu *et al*. 2005). However, for the purpose of simulating the light-adapted state of PSII, various values for the rate constant describing oxidation of PQH_2 at the cytochrome b_6f complex (k_{ox}) were used for reproducing states exhibiting different electron transport sink capacities (i.e. as controlled by downstream metabolism). Moreover, low and high values of k_D ranging from $0.244 * 10^9$ s^{-1} to $5 * 10^9$ s^{-1} were used to simulate variable qN capacities, which correspond approximately to a NPQ ranging from 0 to 9, respectively where NPQ is calculated as Fm/Fm′ – 1 (Stern–Volmer formulation). With the parameterization used for simulations, an irradiance of 1000 μmol m^{-2} s^{-1} corresponds to a rate of excitation of 600 s^{-1} per PSII unit.

Table 1. Rate constants for PSII photochemical reactions used for simulations. The rate constants for decay of excitons by fluorescence (k_F), heat dissipation via basal and non-photochemical (NPQ) processes (k_D), non-radiative decay in reduced and oxidized units (i.e. k_{dred} and k_{dox}, respectively), PSII-mediated electron transfer (K_p), non-photochemical quenching by oxidized PQ (k_{pq}), and inter-unit exciton exchange (k_{UU}) are reported in units of s^{-1}

Rate constant (k)	s^{-1}	Ref.
k_F	$0.056*10^9$	Lavergne and Trissl 1995
k_D	$0.244*10^9$	″
K_{dred}	$2.315*10^8$	[a]
K_{dox}	0	[b]
K_p	$2.654*10^9$	Lavergne and Trissl 1995
k_{pq}	$0.935*10^8$	[c]
k_{UU}	$2*10^9$	[d]

[a]Assumed null; [b]Model estimate retrieved to match $(1 - \Phi_{Fo}/\Phi_{Fm}) = 0.825$ for the dark-adapted value; [c]Model estimate according to Lazar (2003); [d]Model estimate corresponding to a Joliot's connectivity parameter of 0.65 (see Lavergne & Trissl 1995).

RESULTS

MPF dynamics

MPF protocol

Figure 3a shows a plot of a typical MPF comprised of three sequential regimes, or 'phases', of irradiance, each of which can vary in duration and intensity (Q′, μmol $m^{-2}s^{-1}$). The entire MPF sequence occurs within approximately 1 s. Phase 1 is similar to a traditional RF and, in this example, is shown as a step increase in Q′ from the initial actinic PPFD to a plateau. Phase 2 involves a linear decrease in Q′ to a percentage of that attained during phase 1. Herein, the decrease in intensity during phase 2 will be referred to as the ramp depth and is expressed as the fraction by which the maximum phase 1 Q′ is reduced. The absolute rate of decrease in Q′ during phase 2 is referred to as ramp rate and is expressed in mol $m^{-2}s^{-2}$. Both ramp depth and ramp rate are important characteristics of an MPF that will be discussed later. At phase 3, Q′ returns to the phase 1 intensity.

The changes in ΦF during an MPF are also shown in Fig. 3a. The ΦF acquired prior to the MPF corresponds to

Table 2. Rate constants of electron transfer reactions at PSII

k	reaction	s^{-1}	Ref.
k_{AB1}	Q_A^- to Q_B	3500	Baake and Schloder 1992, Lazar 2003
k_{BA1}	Q_B^- to Q_A	175	″
k_{AB2}	Q_A^- to Q_B^-	1750	″
k_{BA2}	Q_B^{2-} to Q_A	35	″
k_3	PQ with Q_B^{2-}	800	Zhu *et al*. 2005
k_{r3}	PQH_2 with Q_B	800	″
k_{ox}	PQH_2 to b_6f	10–350	″

Shown are the values of the rate constants describing the acceptor-side of PSII and that were used during simulations.

Table 3. Concentration and relative stoichiometries

Parameter	Value	Units	Ref.
$[Q_AT] = [Q_A] + [Q_A^-]$	10^{-6}	mol m^{-2}	[a]
n	8	–	Baake and Schloder 1992
N	0.6	–	[b]

Shown are values of total Q_A (Q_AT), the relative size of the plastoquinone pool ($([PQ] + [PQH_2])/([Q_A] + [Q_A^-])$) ($n$), and the fraction of absorbed photons partitioned to PSII (N) that were used for simulations.
[a]Estimate taken from the numbers of chlorophyll molecules per PSII and per unit area; [b]Estimate taken from the number of chlorophyll molecules in PSII relative to PSI, e.g. the relative stoichiometry.

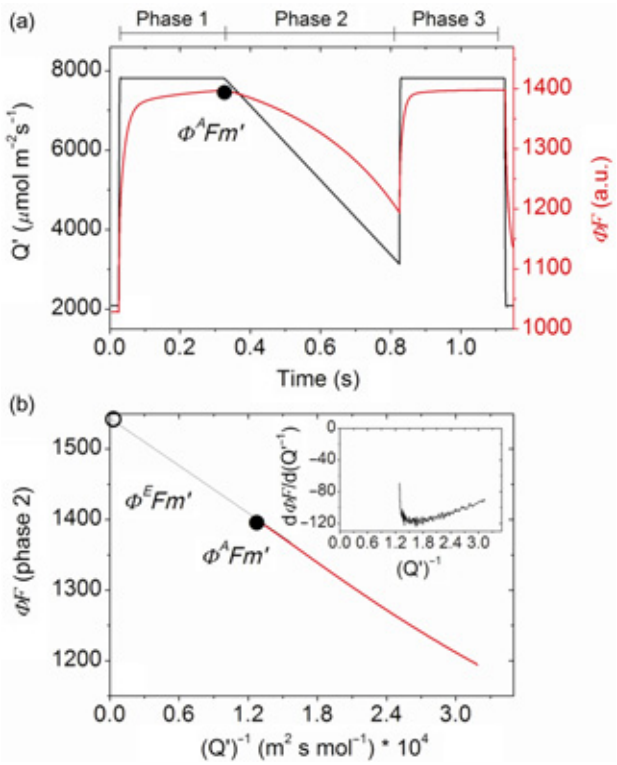

Figure 3. Multiphase flash dynamics used to derive extrapolated Fm′. (a) Changes in flash intensity (Q′) (black) and ΦF (red) are shown during a representative multiphase flash (MPF) applied to a sunflower leaf adapted to 2000 μmol $m^{-2}s^{-1}$. Phase 1 is depicted as an increase in Q′ from 2000 μmol photons $m^{-2}s^{-1}$ to approximately 7800 μmol photons $m^{-2}s^{-1}$ for a duration of 300 ms. The phase 1 intensity was attenuated by 60% during phase 2 for 500 ms, resulting in a ramp rate of 0.0094 mol $m^{-2}s^{-2}$. An absolute value of apparent Fm′ ($\Phi^A Fm'$) of 1392 (arbitrary units, a.u.) was obtained as the ΦF achieved at the end of phase 1 (solid black sphere). (b) ΦF obtained during phase 2 is plotted against $(Q')^{-1}$. Linear regression of ΦF against $(Q')^{-1}$ was performed (thin black line) over the $(Q')^{-1}$ equivalent to the highest 25% in Q′. $\Phi^E Fm'$ was obtained as the intercept of the regression (open sphere), the value of which was 1544 a.u. (i.e. approximately 10% higher than that of $\Phi^A Fm'$). Inset: The first derivative of phase 2 ΦF when plotted versus $(Q')^{-1}$.

steady-state fluorescence. During phase 1, ΦF increases in response to the initial increase in Q′ to an apparent maximum ΦF ($\Phi^A Fm'$) that is a measure of the value that would be obtained using a traditional RF. A hyperbolic decrease in ΦF is observed during phase 2, after which it returns during phase 3 to a level similar to that observed during phase 1. In comparison with the ΦF achieved during phase 1, this recovery of ΦF during phase 3 is diagnostic because deviations between these respective ΦF's may be indicative of auxiliary quenching phenomena that can be induced during the high intensity flash (see Discussion).

The ΦF measured during phase 2 is used to estimate Fm′ at infinite irradiance and will be referred to as Extrapolated Fm′, or $\Phi^E Fm'$. Figure 3b shows ΦF obtained during phase 2 plotted against $(Q')^{-1}$, which is referred to herein as a reciprocal plot. A linear regression of ΦF versus $(Q')^{-1}$ was performed over $(Q')^{-1}$ corresponding to the highest 25% of irradiance during the ramp; the intercept ΦF at $(Q')^{-1} = 0$ yielded a value of $\Phi^E Fm'$ that was ~10% higher than $\Phi^A Fm'$. The regression procedure assumes a linear relationship between ΦF and $(Q')^{-1}$, but the plot is not perfectly linear, as shown by the first derivative of the reciprocal plot (inset of Fig. 3b). The first derivative rapidly reaches a minimum at the beginning of the ramp as the rate of change in ΦF accelerates in response to the ramp in Q′; however, as $(Q')^{-1}$ continues to increase (i.e. Q′ decline) the rate of change in ΦF becomes less negative, reflecting slight upward curvature in the reciprocal plot. Thus, non-linearity in ΦF versus $(Q')^{-1}$ can render estimation of $\Phi^E Fm'$ sensitive to the interval over which the regression is performed. Both ramp depth (see later) and ramp rate can influence the amount of curvature, especially at the beginning of the ramp.

Dependence of fluorescence on irradiance is a function of ramp rate

Simulations

A model (see Materials and Methods) was used to describe the changes in ΦF in response to steady irradiances of variable intensity and to MPF dynamics. A set of time-dependent differential equations was used to simulate both steady values of ΦF and time-dependent solutions, allowing ΦF dynamics comparable with phase 1-to-phase 2 transitions to be studied. The model was run to predict ΦF using specified rate constants describing the capacities for electron transport (i.e. oxidation of PQH_2 at the cytochrome b_6f complex, k_{ox}) and qN (i.e. non-radiative losses in the antenna, k_D). The ΦF obtained at a given steady irradiance simulates phase 1 and corresponds to $\Phi^A Fm'$. Simulations of dynamic changes in ΦF, as occurs during a phase 2 of an MPF, were obtained by decreasing light intensity from a given steady irradiance using a defined rate (i.e. ramp rate, θ) and over a defined range (i.e. ramp depth). $\Phi^E Fm'$ was computed as the intercept of a linear regression of ΦF and $(Q')^{-1}$ over the entire ramp in Q′. Simulated values of ΦF, $\Phi^A Fm'$, and $\Phi^E Fm'$ were normalized to a true value of Fm′, which was simulated at an essentially infinite irradiance (10^6 μmol m^{-2} s^{-1}).

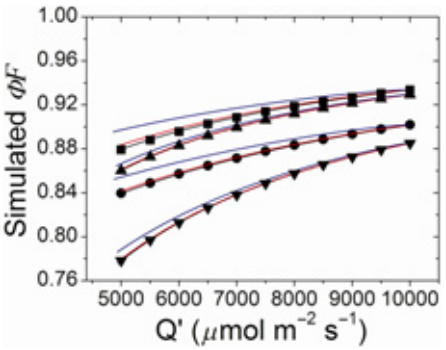

Figure 4. Simulated ΦF in response to Q′ applied as ramp or as steady flashes. Changes in $\Phi^A Fm'$ (symbols) were simulated using steady irradiances between 5000 and 10 000 μmol photons m^{-2} s^{-1}, whereas ΦF's (lines) were simulated over a comparable range of irradiances by attenuating a steady irradiance of 10 000 μmol photons m^{-2} s^{-1} by 50% using ramp rates of 0.01 mol photons m^{-2} s^{-2} (black), 0.1 mol photons m^{-2} s^{-2} (red), and 1 mol photons m^{-2} s^{-2} (blue). Simulations were performed using a range of electron transport and qN capacities by varying k_{ox} and k_D, respectively, according to: $k_{ox} = 50$ s^{-1}; $k_D = 0.244 * 10^9$ s^{-1} (upward triangles and corresponding lines); $k_{ox} = 50$ s^{-1}; $k_D = 5 * 10^9$ s^{-1} (squares and corresponding lines); $k_{ox} = 200$ s^{-1}; $k_D = 5 * 10^9$ s^{-1} (circles and corresponding lines); and $k_{ox} = 200$ s^{-1}; $k_D = 0.244 * 10^9$ s^{-1} (downward triangles and corresponding lines). All values were normalized to the corresponding ΦF at infinite irradiance.

Figure 4 shows simulated saturation light response curves of ΦF in response to Q′ obtained by decreasing irradiance linearly by 50% beginning at 10 000 μmol photons m^{-2} s^{-1} at ramp rates between 0.01 and 1.00 mol photons m^{-2} s^{-2}. The symbols show values of $\Phi^A Fm'$ computed for steady irradiances spanning the same intensity range. These data were collected under four adaptive states by varying the rate constants for electron transport and qN capacities. Under all adaptive states, there is close correspondence between the ΦF's obtained using steady irradiances and those obtained while varying Q′ at ramp rates between 0.01 and 0.10 mol photons m^{-2} s^{-2}; however, the ΦF obtained using a ramp rate of 1 mol m^{-2} s^{-2} was consistently higher than the estimates of $\Phi^A Fm'$ computed using steady irradiances over all Q′ and adaptive states.

The effect of ramp rate on estimation of $\Phi^E Fm'$ is shown in Fig. 5. Regardless of the adaptive state, comparison of $\Phi^E Fm'$ measured at a ramp rate of 0.001 mol photons m^{-2} s^{-2} to $\Phi^E Fm'$ measured at faster rates shows that it tends to decline as ramp rate increases, but the decline is negligible at rates of 0.01 mol m^{-2} s^{-2} or lower, and constrained to approximately 0.5% or less at rates below 0.1 mol m^{-2} s^{-2}.

Experiments

Experiments confirm that ramp rate is an essential characteristic of an MPF that can impact the value of $\Phi^E Fm'$. Figure 6 shows phase 2 ΦFs that were obtained using MPFs with maximum phase 1 intensities of approximately 7800 μmol m^{-2} s^{-1} and ramps of 25% at two different rates. Also shown are estimates of $\Phi^A Fm'$ that were measured during a series of RFs that spanned an intensity range

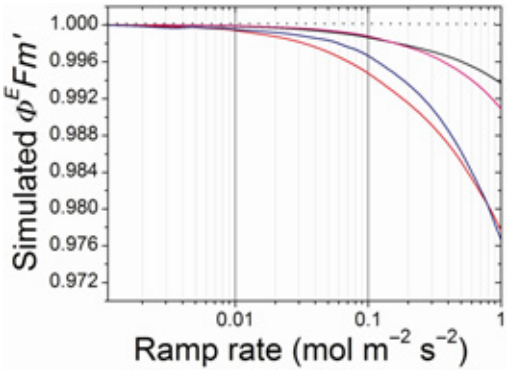

Figure 5. Simulated effect of ramp rate on $\Phi^E Fm'$. Estimates of $\Phi^E Fm'$ were simulated by attenuating a steady irradiance of 10 000 μmol photons m^{-2} s^{-1} by 25% using a range of ramp rates between 0.001 and 1.000 mol photons m^{-2} s^{-2}. The ΦF achieved during the ramp phase was plotted against $(Q')^{-1}$ and estimates of $\Phi^E Fm'$ were obtained by linear regression and extrapolation to the *y*-intercept. Simulations were performed over a range of electron transport and qN capacities by varying k_{ox} and k_D, respectively, according to: $k_{ox} = 50$ s^{-1}, $k_D = 0.244 * 10^9$ s^{-1} (black), $k_{ox} = 200$ s^{-1}, $k_D = 0.244 * 10^9$ s^{-1} (magenta), $k_{ox} = 50$ s^{-1}, $k_D = 5 * 10^9$ s^{-1} (red), $k_{ox} = 200$ s^{-1}, $k_D = 5 * 10^9$ s^{-1} (blue). Each data set at a given electron transport and qN capacity was normalized to the values of $\Phi^E Fm'$ that were obtained using the slowest ramp rate of 0.001 mol photons m^{-2} s^{-2}. These values of $\Phi^E Fm'$ were, in order of the abovementioned adaptive capacities, 0.9991, 0.9952, 0.9927 and 0.9756.

comparable with that which occurred during phase 2 of the MPF's. At the slower ramp rate (0.0078 mol photons m^{-2} s^{-2}), close correspondence is observed between ΦF and the series of values of $\Phi^A Fm'$ over the entire range of Q′. The resulting slopes of ΦF plotted against $(Q')^{-1}$ obtained during the MPF's and those obtained from the series of discrete $\Phi^A Fm$s were identical (data not shown), resulting in estimates of $\Phi^E Fm'$ that were statistically indistinguishable. Based on the faster MPF ramp rate (0.094 mol photons m^{-2} s^{-2}), ΦF was consistently higher than both the ΦF obtained at the slower ramp rate and the values of $\Phi^A Fm'$ based on a series of RFs. Consequently at the faster ramp rate, the slope of ΦF against $(Q')^{-1}$ was more shallow than the corresponding slope based on the slower ramp rate (data not shown), causing estimates of $\Phi^E Fm'$ to be about 3% lower. Similar results were observed at different background actinic-light levels, and for leaves of different species (data not shown).

Effect of ramp depth on estimation of $\Phi^E Fm'$

Simulations

Figure 7a shows simulated phase 2 ΦF's plotted against $(Q')^{-1}$. The plots exhibit subtle curvature, which was quantified by calculating the first derivatives of the reciprocal plots (Fig. 7b). At ramp rates of 0.01 mol photons m^{-2} s^{-2} and 0.1 mol photons m^{-2} s^{-2}, the values of the derivatives quickly reached minima, after which they became progressively less negative in a manner similar to the experimental data (Fig. 3b, inset). The initial accelerating declines in slopes, which reflect the initial (i.e. at the highest irradiances) downward curvatures of the reciprocal plots, were reduced or eliminated at slower ramp rates. The derivative based on a slow ramp rate of 10^{-5} mol m^{-2} s^{-2} was less complex and simply became progressively less negative from the highest to the lowest irradiances, because the corresponding reciprocal plot was hyperbolic and characterized entirely by upward curvature.

Because $\Phi^E Fm'$ is estimated by linear regression and extrapolation of reciprocal plots that have some curvature, there is potential for estimates of $\Phi^E Fm'$ to vary as a function of ramp rate and ramp depth. At ramp rates of 0.01 mol photons m^{-2} s^{-2} and 0.1 mol photons m^{-2} s^{-2}, simulated estimates of $\Phi^E Fm'$ increased when ramp depths increased from 4 to 20%, albeit by less than one percent (Fig. 7c), as the derivative is less negative (i.e. slope less steep) at the beginning of the curve (Fig. 7b). The increase in $\Phi^E Fm'$ with the shorter ramps was completely eliminated at the slowest ramp rate of 10^{-5} mol m^{-2} s^{-2}. At the slowest ramp rate, estimates of $\Phi^E Fm'$ gradually decreased as a function of increasing ramp depth, as shown by the derivative becoming continuously less negative as the slope of ΦF versus $(Q')^{-1}$ gets shallower.

Simulated estimates of $\Phi^E Fm'$ vary as a function of ramp depth over a range of adaptive states. Figure 8 shows simulated estimates of $\Phi^E Fm'$ plotted against increasing ramp depth between 4 and 50% and using a constant ramp rate of 0.01 mol m^{-2} s^{-2}. Depending upon the adaptive condition, the

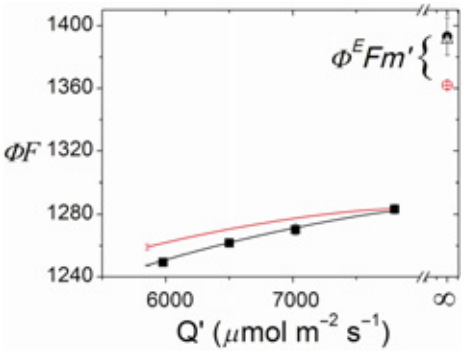

Figure 6. ΦF measured with the multiphase flash (MPF) protocol and $\Phi^A Fm'$ measured with a series of rectangular flashes (RFs). Three sequences of four RFs and two MPFs were applied in randomized order to a sunflower leaf adapted to an actinic photon flux density (PPFD) of 2000 μmol m^{-2} s^{-1}. Pulses within a given sequence were separated by 1 min. $\Phi^A Fm'$ values (squares) were measured using four, variably intense RFs that were 900 ms in duration and spanned intensities between approximately 5700 μmol m^{-2} s^{-1} and 7800 μmol m^{-2} s^{-1}. Using MPFs that differed in ramp rate, estimates of phase 2 ΦFs (lines) were measured by attenuating phase 1 intensities of 7800 μmol m^{-2} s^{-1} by 25% at ramp rates of 0.094 mol m^{-2} s^{-2} (red) and 0.0078 mol m^{-2} s^{-2} (black). Estimates of $\Phi^E Fm'$ were obtained by linear regression and extrapolation of $\Phi^A Fm'$ and ΦF versus $(Q')^{-1}$. $\Phi^E Fm'$ (RF-derived) (circle): 1388 ± 12; $\Phi^E Fm'$ (MPF-derived using 0.0078 mol m^{-2} s^{-2}) (triangle): 1386 ± 2; $\Phi^E Fm'$ (MPF-derived using 0.094 mol m^{-2} s^{-2}) (red hexagon): 1363 ± 3. Error bars correspond to± SD of the mean of three replications on a single sunflower leaf. Data are representative of leaves of three plants.

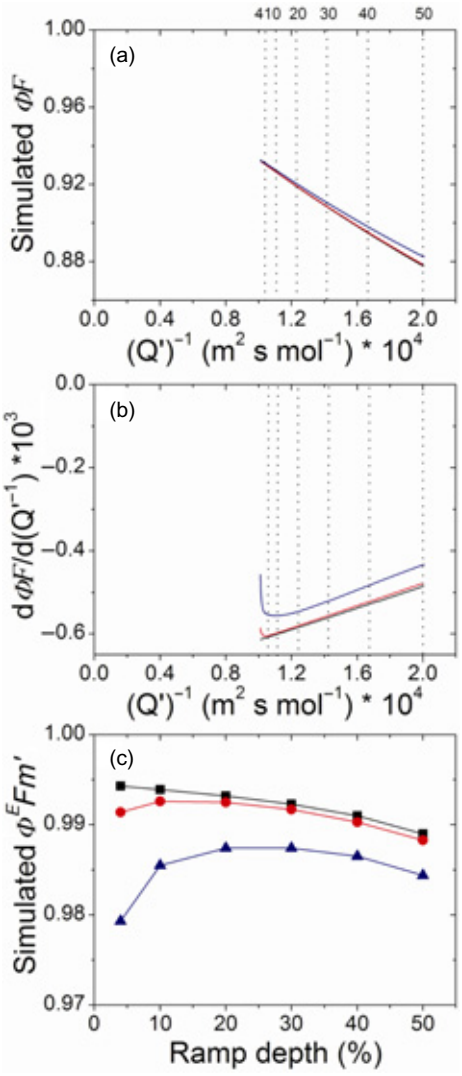

Figure 7. Simulated ΦF's, their derivatives and estimates of $\Phi^E Fm'$. (a) ΦF's were simulated using a single adaptive capacity (i.e. $k_{ox} = 50\ s^{-1}$; $k_D = 5 * 10^9\ s^{-1}$) by attenuating a steady irradiance of 10 000 μmol $m^{-2}\,s^{-1}$ by 50% at 10^{-5} mol $m^{-2}\,s^{-2}$ (black), 0.01 mol $m^{-2}\,s^{-2}$ (red), and 0.10 mol $m^{-2}\,s^{-2}$ (blue) and are shown plotted against $(Q')^{-1}$. Vertical, dotted lines from left-to-right are values of $(Q')^{-1}$ corresponding to saturation pulse irradiances (Q′) that are 4, 10, 20, . . ., 50% lower than the maximum steady irradiance of 10 000 μmol $m^{-2}\,s^{-1}$. (b) The first derivatives of the reciprocal plots in Panel A were calculated to quantify their curvatures. The line colours and vertical dotted lines are as described in Panel A. (c) A steady irradiance of 10 000 μmol $m^{-2}\,s^{-1}$ was attenuated by 50% and a range of estimates of $\Phi^E Fm'$ were obtained by performing a series of linear regressions and extrapolations of the resultant plot of ΦF versus $(Q')^{-1}$, always starting the regressions at the highest irradiance and extending them over progressive decreases in the maximum irradiance by between 4 and 50%. ΦF's were obtained using an adaptive state corresponding to $k_{ox} = 50\ s^{-1}$, $k_D = 5 * 10^9\ s^{-1}$ and ramp rates of 0.1 mol $m^{-2}\,s^{-2}$ (blue triangles), 0.01 mol $m^{-2}\,s^{-2}$ (red circles), and 10^{-5} mol $m^{-2}\,s^{-2}$ (black squares). The values of ΦF were normalized to the corresponding values at infinite irradiance.

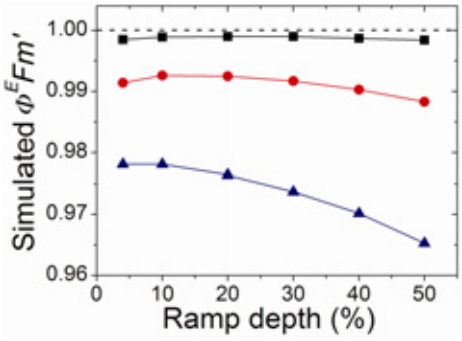

Figure 8. Simulated effect of ramp depth on estimation of $\Phi^E Fm'$ under variable adaptive states. A range of simulated estimates of $\Phi^E Fm'$ were obtained (i.e. as described in the legend of Figure 7) by ramping 10 000 μmol $m^{-2}\,s^{-1}$ at a constant rate of 0.01 mol $m^{-2}\,s^{-2}$ over ramp depths ranging between 4 and 50%. Three different electron transport and qN capacities were used during simulations by varying k_{ox} and k_D, respectively, according to: $k_{ox} = 50\ s^{-1}$; $k_D = 0.244 * 10^9\ s^{-1}$ (black squares); $k_{ox} = 50\ s^{-1}$; $k_D = 5 * 10^9\ s^{-1}$ (red circles); and $k_{ox} = 200\ s^{-1}$; $k_D = 5 * 10^9\ s^{-1}$ (blue triangles). All values were normalized to corresponding ΦF at infinite irradiance.

values of $\Phi^E Fm'$ remain more or less constant between ramp depths of 4 and 20%, following, which they only gradually decrease, but by no more than approximately 1%, out to a ramp depth of 50%.

Experiments

Experimental estimates of $\Phi^E Fm'$ can vary as a function of the ramp depth (Fig. 9). Compared with maximum $\Phi^E Fm'$ obtained with a ramp depth of 20%, estimates of $\Phi^E Fm'$ are

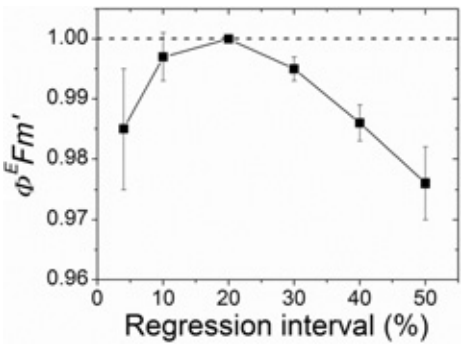

Figure 9. Experimental effect of ramp depth on estimation of $\Phi^E Fm'$. MPF's comprised of maximum phase 1 intensities of 7700–8000 μmol $m^{-2}\,s^{-1}$ were applied to sunflower leaves adapted to 1500 μmol $m^{-2}\,s^{-1}$ for 45–50 min. The phase 1 intensities were attenuated by 60% during phase 2 at rates of 0.018 mol $m^{-2}\,s^{-2}$. A range of estimates of $\Phi^E Fm'$ were obtained by performing a series of linear regressions and extrapolations of the plot of ΦF versus $(Q')^{-1}$, always starting the regressions at the highest irradiance and extending them over progressive decreases in the maximum irradiance by between 4 and 50%. All values have been normalized to the value of $\Phi^E Fm'$ obtained at a ramp depth of 20%. Each point is the mean ± SD of n = 7.

shown to increase by approximately 1.5% as ramp depth increases from approximately 4–20%; they remain within about 0.5% between ramp depths of 10–30%; following which they gradually decrease by 2.0–2.5% over ramp depths of 30–50%. Similar results were obtained using different background actinic-light levels and leaves from multiple species (data not shown). These combined results are consistent with the presence of modest sigmoidal curvature within the plots of ΦF versus $(Q')^{-1}$ (data not shown), essentially as seen in Fig. 3b and in simulations (Fig. 7). In addition, the amplitude of the increase in $\Phi^E Fm'$ at short ramp depths, an effect which is due to the initial downward curvature of the plot of ΦF versus $(Q')^{-1}$, was sensitive to ramp rate (data not shown) in a manner that was similar to that observed in simulations (Fig. 7c).

Dependence of $\Phi^A Fm'$ and $\Phi^E Fm'$ on Q′

Simulations

Simulated estimates of $\Phi^E Fm'$ are invariably closer than $\Phi^A Fm'$ as approximations of Fm′. Under all electron transport and qN capacities, simulated estimates of $\Phi^A Fm'$ varied between 0.84 and 0.94 from the lowest to the highest steady irradiances, respectively, while the corresponding values of $\Phi^E Fm'$ were between 0.92 and 0.99 (Supporting Information Fig. S1). In all conditions simulated, estimates of $\Phi^E Fm'$ were always closer than $\Phi^A Fm'$ to unity, regardless of the starting value of Q′ or the adaptive state.

Experimental observations

Experimental estimates of $\Phi^E Fm'$ are systematically higher and less dependent on Q′ than those of $\Phi^A Fm'$ (Fig. 10). Compared with $\Phi^E Fm'$ obtained at 13 000 μmol m^{-2} s^{-1}, estimates of $\Phi^A Fm'$ increased from approximately 0.83–0.93 from the lowest to the highest Q′, respectively. In contrast, the corresponding values of $\Phi^E Fm'$ varied from approximately 0.96–0.99 and they remained more or less constant from 7000 to 13 000 μmol m^{-2} s^{-1}. In all leaves tested, including leaves both from multiple species and adapted to different background actinic-light levels (data not shown), estimates of $\Phi^E Fm'$ were always larger than those of $\Phi^A Fm'$ and were less variable with Q′.

Differences between estimates of $\Phi^A Fm'$ achieved during phases 1 and 3 varied with species. Estimates of $\Phi^A Fm'$ obtained during phases 1 and 3 using sunflower leaves varied by less than a single percent (Fig. 10) and the differences were even smaller in other sunflower leaves tested (data not shown). In maize and bean leaves, while differences in estimates of $\Phi^A Fm'$ achieved during phases 1 and 3 were quite small at lower pulse intensities, the differences progressively increased as a function of increasing pulse intensity (data not shown), possibly indicative of auxiliary reactions induced during the pulses (see Discussion).

Application of MPF for estimation of J and g_m

MPF-derived values of $\Phi^E Fm'$ can compensate for underestimation of Fm′ that can occur using standard RFs and can

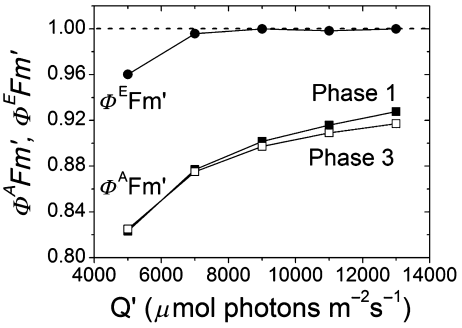

Figure 10. Saturation pulse-dependence of $\Phi^A Fm'$ and $\Phi^E Fm'$ in an intact leaf. A sunflower leaf was adapted to 2000 μmol m^{-2} s^{-1}, after which a series of MPFs that varied in phase 1 intensities (i.e. Q′) between 5000 and 13 000 μmol m^{-2} s^{-1} was applied in a randomized manner. Estimates of $\Phi^A Fm'$ (closed squares) were taken as the maximum ΦF achieved at the end of phase 1, the duration of which was 300 ms. The phase 1 intensities were attenuated by 20% at rates of 0.0087 mol m^{-2} s^{-2} during phase 2 and estimates of $\Phi^E Fm'$ (closed circles) were derived via linear regression and extrapolation of the phase 2 ΦF's plotted against $(Q')^{-1}$. The values of $\Phi^A Fm'$ achieved at the end of the 300 ms phase 3 are also shown (open squares). All data have been normalized to the maximum value of $\Phi^E Fm'$ obtained at 13 000 μmol m^{-2} s^{-1}.

therefore impact the values of derived parameters such as J and g_m. Figure 11 shows light curves of the parameters required to estimate J that were obtained in maize and sunflower leaves adapted to a range of actinic PPFDs. The values of $\Phi^E Fm'$ were invariably higher than the corresponding estimates of $\Phi^A Fm'$ in both maize and sunflower (Fig. 11a,d). In maize, estimates of $\Phi^E Fm'$ were approximately 14% and approximately 20% higher than those of $\Phi^A Fm'$ at the lowest and highest PPFD's, respectively, and a similar pattern was observed for sunflower. As a result, $\Phi^E Fm'$-derived estimates of Φ_{PSII} in maize and sunflower were, as a function of increasing PPFD, progressively higher by 6–31% and 5–20%, respectively, than their $\Phi^A Fm'$-derived counterparts (Fig. 11b,e). Consequently, estimates of J based on $\Phi^E Fm'$-derived values of Φ_{PSII} in both maize and sunflower were, as a function of increasing PPFD, progressively higher than their $\Phi^A Fm'$-derived counterparts (Fig. 11c,f). It is also noteworthy that in both maize and sunflower, estimates of J based on $\Phi^E Fm'$-derived values of Φ_{PSII} did not exhibit saturation, in contrast to the corresponding $\Phi^A Fm'$-derived values of J.

The relationship between J and A_G is sensitive to whether J is calculated from $\Phi^A Fm'$- or $\Phi^E Fm'$-derived values of Φ_{PSII} (Fig. 12). Based on data collected in maize, the intercept of a linear regression between A_G and estimates of J based on $\Phi^E Fm'$-derived values of Φ_{PSII} was statistically indistinguishable from zero and the slope was 4.7 electrons per CO_2. In contrast, linear regression of the relationship when J was estimated using $\Phi^A Fm'$-derived values of Φ_{PSII} resulted in an intercept that was statistically different from zero and the slope was 2.9 electrons per CO_2.

Estimates of g_m by the variable J method (Harley *et al.* 1992) were significantly affected by whether J was estimated

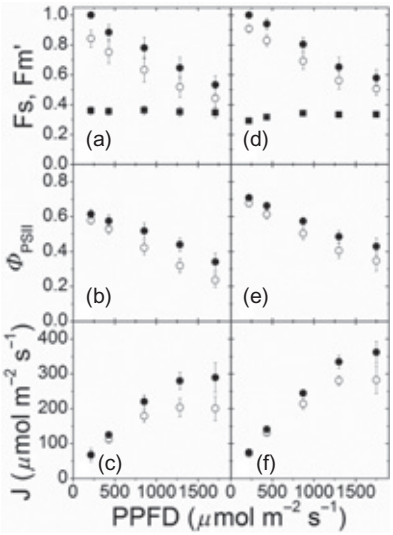

Figure 11. Fluorescence light response curves measured in leaves of field-grown plants. Fluorescence parameters needed to calculate J were estimated in maize (a–c) and sunflower (d–f) leaves adapted to actinic photon flux density's (PPFD) ranging between 200 and 1800 μmol m^{-2} s^{-1}. Fluorescence yields in Panels A and D are mean normalized values of *F* (squares) and Fm′ (i.e. either $\Phi^A Fm'$ or $\Phi^E Fm'$; see later) at each absorbed PPFD; each point was normalized to $\Phi^E Fm'$ at the lowest PPFD to correct for leaf to leaf variability in fluorescence yield. Estimates of $\Phi^A Fm'$ were obtained using traditional rectangular flashes (RFs) of 8000 μmol m^{-2} s^{-1} (open circles). MPF's comprised of phase 1 intensities of ~8000 μmol m^{-2} s^{-1} were attenuated by 30% at rates of 0.01 mol m^{-2} s^{-2} in order to obtain the ΦF's that were used to estimate values of $\Phi^E Fm'$ by linear regression of the ΦF's versus $(Q')^{-1}$ and extrapolation to the *y*-intercept. The data in Panels B and E show the resulting values of Φ_{PSII} that were calculated using the estimates of $\Phi^A Fm'$ and $\Phi^E Fm'$ (i.e. open and filled circles, respectively). Panels C and F show estimates of J that were computed using the respective $\Phi^A Fm'$-derived and $\Phi^E Fm'$-derived values of Φ_{PSII} (i.e. open and filled circles, respectively). Each maize data point is the mean of nine to 14 observations (± SD), and each sunflower data point is the mean of seven to nine observations (± SD). Paired comparisons of the mean normalized differences between the MPF and RF methods were significant ($P < 0.01$) at all PPFD.

by $\Phi^A Fm'$- or $\Phi^E Fm'$-derived values of Φ_{PSII} (Table 4). Using sunflower, estimates of g_m based on $\Phi^E Fm'$-derived values of J remained constant at approximately 0.5 mol m^{-2} s^{-1} bar^{-1} over the range of PPFD and the standard deviations were 22–29% of the means. In contrast, $\Phi^A Fm'$-derived estimates of g_m were highly erratic and ranged between 1.47 and –2.43 mol m^{-2} s^{-1} bar^{-1} over the same range of PPFD. It is important to note that the standard deviations of the $\Phi^A Fm'$-derived values of g_m were observed to progressively increase as a function of increasing PPFD and in some cases the variability exceeded several hundred percent of the means. That these extreme differences between $\Phi^E Fm'$- and $\Phi^A Fm'$-derived estimates of g_m directly reflect differences in the corresponding estimates of J (Fig. 11) is supported by the fact that the estimates of net CO_2 assimilation (A_n) and intercellular [CO_2] (C_i), both of which also serve as input variables in the g_m equation, were not different between RF and MPF treatments (Table 4).

DISCUSSION

Determination of Fm′ using a multiturnover approach for saturating PSII photochemistry requires complete reduction of Q_A and PQ pools, which is a redox state that may be difficult to achieve, even when using extreme pulse intensities (Markgraf & Berry 1990). Several groups have shown that $\Phi^A Fm'$ increases hyperbolically towards an asymptote as a function of increasing Q′ (Markgraf & Berry 1990; Earl & Ennahli 2004). As a result, values of $\Phi^A Fm'$ at the higher irradiances exhibit linearity when plotted against $(Q')^{-1}$, providing the basis for obtaining approximations of Fm′ at infinite irradiance (i.e. true Fm′) by linear regression and extrapolation to the zero intercept (Markgraf & Berry 1990). In effect, the extrapolated value of Fm′, or $\Phi^E Fm'$, can compensate for underestimation of Fm′ that often occurs because of acceptor turnover at PSII. Herein we present a new MPF approach that is capable of measuring the hyperbolic changes in ΦF that occur while rapidly attenuating the maximum Q′ during a single flash. In principle, the MPF approach and that proposed by Markgraf and Berry (1990) are comparable in the sense that both measure the dependency of $\Phi^A Fm'$ versus $(Q')^{-1}$, which is then used to estimate $\Phi^E Fm'$. The primary difference is that the MPF approach is capable of doing so within 1 s, instead of over a period of several minutes, which is required when using several flashes of variable intensity (Markgraf & Berry 1990). The basis of the MPF approach is that under

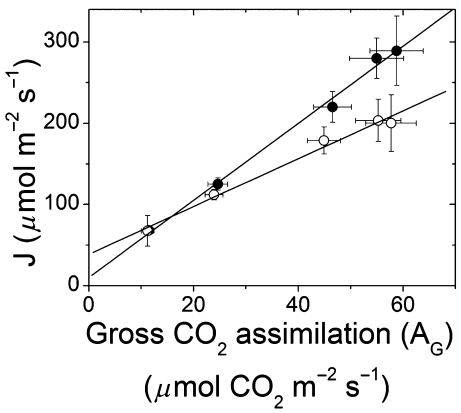

Figure 12. Comparative analysis of fluorescence and gas exchange in field-grown maize. Estimates of J were calculated from values of Φ_{PSII} obtained using either $\Phi^A Fm'$ or $\Phi^E Fm'$ (see Figure 11 legend), based on rectangular flashes (RFs; open) and MPF (filled) methods and are plotted as a function of gross CO_2 assimilation rate (A_G). Each data point is the mean of nine to 14 observations (± SD). The parameters based on a linear fit ($y = bx + y_0$) of the data set obtained using the RFs were: $y_0 = 38.7 \pm 7.7$ and $b = 2.9 \pm 0.2$ and an r^2 of 0.989. The intercept was found to significantly differ from zero ($P = 0.015$). The corresponding parameters based on the MPF-derived estimates of J were: $y_0 = 10.2 \pm 8.9$ and $b = 4.7 \pm 0.2$ and an r^2 of 0.994. The intercept did not significantly differ from zero ($P = 0.337$).

Table 4. Gas exchange parameters for estimating mesophyll conductance

	RF				MPF			
PPFD (μmol m^{-2} s^{-1})	A_n (μmol m^{-2} s^{-1})	g_s (mol m^{-2} s^{-1})	C_i (μbar)	g_m (mol m^{-2} s^{-1} bar^{-1})	A_n (μmol m^{-2} s^{-1})	g_s (mol m^{-2} s^{-1})	C_i (μbar)	g_m (mol m^{-2} s^{-1} bar^{-1})
873	32.2 ± 0.8	0.43 ± 0.08	284 ± 6	1.47 ± 1.02	32.0 ± 1.2	0.42 ± 0.07	283 ± 8	0.51 ± 0.12
1378	39.2 ± 2.8	0.48 ± 0.08	275 ± 10	1.52 ± 3.49	39.1 ± 2.8	0.47 ± 0.08	274 ± 10	0.49 ± 0.14
2000	42.8 ± 2.6	0.51 ± 0.08	271 ± 10	-2.4 ± 11.5	42.8 ± 2.4	0.51 ± 0.08	271 ± 10	0.50 ± 0.11

Light curves of gas exchange and fluorescence parameters were measured using Sunflower leaves in order to determine mesophyll conductance (g_m) by the variable J method according to Harley *et al.* (1992) using a value of Γ^* of 51 μmol mol^{-1} for our measurement temperature (30.3°C ± 0.16). This temperature-corrected value was estimated according to von Caemmerer (2000) from reported C* obtained at 23°C for sunflower (Vrabl *et al.* 2009) as $\Gamma^* = C^* + R_d/g_m$ where C* is C_i at which $A_n = -R_d$. R_d was 0.7 μmol m^{-2} s^{-1}. All values represent means ± SD for $n = 5$ leaves.

specified circumstances, the response of ΦF to changing Q′ is the same whether Q′ varies continuously during phase 2 of an MPF, or is provided as a series of steady flashes spanning the same intensity range.

We examined this issue both experimentally and with a comprehensive model (Materials and Methods) that simulated fluorescence dynamics from the kinetics of PSII photochemistry and downhill electron transport on the acceptor side of PSII. Over a range of adaptive states, simulations demonstrated that when the rate of change in Q′ was no greater than 0.01 mol photons m^{-2} s^{-2} (Fig. 4), ΦF was essentially the same function of irradiance whether Q′ was attenuated continuously, as in phase 2 of an MPF, or was varied over the same intensity range as a series of discrete simulations, each being run to steady state at a different constant irradiance. Similar results were obtained experimentally. In experiments with ramp rates <0.01 mol photons m^{-2} s^{-2} (Fig. 6), extrapolated Fm′ values were statistically indistinguishable from those derived from a series of steady irradiance pulses over the same range of intensities. This suggests ΦF remained in quasi-steady-state with respect to irradiance when rates of change in irradiance were sufficiently slow, that is at or below 0.01 mol photons m^{-2} s^{-2}.

By contrast, quasi-steady state could not be maintained when phase 2 attenuation rates exceeded 0.01 mol photons m^{-2} s^{-2}. Under these conditions simulated Q_A^- and PQH_2 pools were elevated above their corresponding steady state values (data not shown) indicating that re-oxidation lagged behind the changing irradiance; this caused (1) fluorescence yields to be elevated compared with those expected at equivalent steady state irradiances, as observed in Fig. 4; (2) the slopes of the reciprocal plots to be shallower than expected (data not shown); and (3) extrapolated Fm′ to be underestimated, as observed at high ramp rates (Fig. 5). Similar results were observed in experiments (Fig. 6); ΦF was elevated and $\Phi^E Fm'$ was underestimated when the ramp rate exceeded 0.01 mol photons m^{-2} s^{-2}.

Therefore, both simulations and experiments demonstrate that when appropriate ramp rates are used, fluorescence yields remain in quasi-steady state with respect to changing irradiance, and estimates of extrapolated Fm′ are essentially the same whether they were obtained by the MPF method or from a series of steady irradiances.

Dependence of ΦF on Q′ during a ramp

The relationships between ΦF and $(Q')^{-1}$ obtained using appropriate irradiance attenuation rates can be extrapolated to estimate Fm′, but they were never truly linear in either our experiments or simulations. Slight sigmoidal curvature was evident in plots of ΦF versus $(Q')^{-1}$ derived by the MPF method and we suggest this is due to the combined effects of two phenomena. One is kinetic, and sensitive to ramp rate, and the other is due to the intrinsic hyperbolic nature of the steady-state response of fluorescence to irradiance. The effects of both phenomena can be minimized by using appropriate experimental conditions.

The kinetic effect can be seen experimentally in Fig. 3b as a slight downward curvature at the beginning (i.e. starting at the highest irradiance) of the plot of ΦF versus $(Q')^{-1}$. This can be seen more clearly in the inset of Fig. 3b as a sharp decrease in the value of the first derivative at high irradiance. Simulations showed similar behaviour (Fig. 7a,b) at higher Q′ attenuation rates, but the slight downward curvature of the reciprocal plot could be completely eliminated as the ramp rate approached zero (Fig. 7a,b). This suggests the initial shallower slopes in plots of ΦF versus $(Q')^{-1}$ arise because Q′ changes almost instantaneously at the onset of the ramp phase, while a finite period of time is required for the acceptor pools in PSII (i.e. Q_A and PQ) to respond to changing light level. The kinetic inertia of acceptor pool turnover may account for the sharp acceleration towards steeper slopes of ΦF in response to changing Q′. The period over which the derivative decreases represents the time required for ΦF to come into quasi-steady state with respect to the changing light level. The relationship of ΦF to $(Q')^{-1}$ during this initial period likely depends on the number and size of interacting pools and their rates of turnover in relation to the rate of decline in Q′. This effect is magnified at higher ramp rates and explains why the extrapolated values of Fm′ initially may increase with ramp depth (Figs 7c & 9) when ramp depths are below approximately 10%. The effects of this slight downturn are largely eliminated by using appropriate ramp rates and ramp depths ≥10% of the starting pulse intensity.

Beyond the kinetic effect, both simulated and experimental reciprocal plots go through an inflection point and are characterized by slight upward hyperbolic curvature as Q′

continues to decline (Figs 3b & 7a); this accounts for the observation that extrapolated Fm′ progressively decreases at larger ramp depths (Figs 7c, 8, & 9). This curvature is present because the underlying relationship of ΦF to SP intensity shows hyperbolic saturation. The difference between plots of ΦF versus Q′ and ΦF versus $(Q')^{-1}$ is simply the difference between moving towards saturation and moving away from saturation, respectively. When leaves are easy to saturate and ΦF is near saturation (e.g. low k_{ox} and low k_D), plots of ΦF versus $(Q')^{-1}$ exhibit only slight upward curvature (Fig. 7), rendering estimates of extrapolated Fm′ less sensitive to ramp depth, as the simulations show (Figs 7c, 8 & Supporting Information Fig. S1). When leaves are harder to saturate and ΦF is farther from saturation (e.g. high k_{ox} and high k_D), plots of ΦF versus $(Q')^{-1}$ exhibit more pronounced curvature, rendering estimation of extrapolated Fm′ more sensitive to ramp depth (Figs 7c, 8 & Supporting Information Fig. S1). This hyperbolic curvature is intrinsic to the response of ΦF to Q′ and results from the convolution of two relationships: (1) the hyperbolic relationship between Q_A redox state and Q′ and (2) the hyperbolic relationship between the variable fraction of ΦF and the redox state of Q_A, which is function of the exciton connectivity between PSII units (Joliot & Joliot 1964, Lavergne & Trissl, 1995). Actually, in the absence of NPQ, it is largely component (2) that explains why it is difficult to saturate ΦF at high irradiances when Q_A is close to fully reduced state (e.g. low k_{ox} and low k_D, see Supporting Information Fig. S2). In contrast, in the presence of NPQ, component (2) becomes less influential and component (1) is predominantly determinative of the relationship between ΦF and Q′ (e.g. low k_{ox} and high k_D, see Supporting Information Fig. S2).

In the MPF method, the apparent linearity of ΦF versus $(Q')^{-1}$ should be viewed simply as a limiting case of an underlying hyperbolic relationship. The effects of non-linearity on attenuating the relative value of $\Phi^E Fm'$ can be largely avoided by limiting ramp depths to ≤30% of the starting pulse intensity, although the optimal range may vary with plant species and conditions. The apparent rigorous linearity reported previously by Earl & Ennahli (2004) and Markgraf and Berry (1990) was likely due to limitations in the ability of sparse data sets to resolve subtle deviations from linearity. An advantage of the MPF approach is that it gives much higher data resolution than previous approaches that relied on a few discrete SP intensities.

Setting up the parameters of MPF

Results from both simulations and experiments show that the effects of slight non-linearities are small when appropriate ramp rates and ramp depths are chosen. In simulations, when ramp rate was ≤0.01 mol $m^{-2} s^{-2}$, extrapolated Fm′ was within about 1% of the true value in all adaptive states (Figs 4 & 8), except when k_D and k_{ox} were both high, which rarely occurs in nature. In experiments, good results were obtained when ramp rates were below 0.01 mol $m^{-2} s^{-2}$ and ramp depths were 10–30% of the pulse irradiance. Under these conditions, variations in extrapolated Fm′ with ramp depth were well constrained (Figs 6 & 9). Thus, we obtain good results when the following criteria are met:

$$0.01 \geq \frac{Q'_{max} D}{\Delta t}$$

and

$$0.1 \leq D \leq 0.3$$

where Q'_{max} is the value of Q′ at the end of phase 1 (mol $m^{-2} s^{-1}$; *note the units:* moles of photons, *not* μmol), D is ramp depth as a fraction of SP irradiance, and Δt is duration of the ramp (seconds; duration of Phase 2 of the MPF). Our experimental data suggest that ideally Q'_{max} should be ≥7000 μmol $m^{-2} s^{-1}$; however, errors in $\Phi^E Fm'$ are well constrained when starting from lower saturating Q′ and, in any case, $\Phi^E Fm'$ was a better estimator of Fm′ than $\Phi^A Fm'$ for all saturating Q′ tested. We recommend that a preliminary assessment of the effects of varying Q′ be performed similar to Fig. 10 for the species of interest prior to beginning an experimental program.

The MPF method provides better estimates of Fm′ and photosynthetic parameters

Simulations show that $\Phi^E Fm'$ invariably out performed $\Phi^A Fm'$ as a proxy of true Fm′, regardless of the initial maximum Q′ or the adaptive state (Supporting Information Fig. S1). The accuracy of $\Phi^E Fm'$ as an estimator of true Fm′ can be discussed in the context of two independent lines of experimental evidence. First, estimates of $\Phi^E Fm'$ were nearly constant with increases in Q′ over a range of approximately 7000 to 13000 μmol photons $m^{-2} s^{-1}$, whereas values of $\Phi^A Fm'$ not only progressively increased over this same range of pulse irradiances, but also were invariably lower than $\Phi^E Fm'$ (Fig. 10). Historically, constancy of $\Phi^A Fm'$ upon increasing the pulse irradiance (*i.e.* saturation) has been used as a test criterion for achieving true Fm′. By this criterion, these results imply that $\Phi^E Fm'$ alone is the accurate estimator of Fm′. Secondly, estimates of J based on $\Phi^E Fm'$-derived values of Φ_{PSII} and A_G exhibited a linear relationship in which the intercept of the regression was statistically indistinguishable from zero and the slope was 4.7 electrons per CO_2 fixed (Fig. 12), essentially as predicted from theory (Genty *et al.* 1989; Krall & Edwards 1990, 1992). In contrast, when J was computed using Φ_{PSII} derived from $\Phi^A Fm'$, the intercept of the linear relationship of J and A_G was significantly greater than zero and the slope substantially underestimated the electron requirement per CO_2 expected from theory (Fig. 12). These results indicate that only the $\Phi^E Fm'$-derived estimates of J are accurate over this wide range of PPFD's, implying that estimates of $\Phi^E Fm'$ are better proxies of true Fm′. This conclusion can impact Fm′-derived parameters other than just Φ_{PSII} and J, for example qN-related parameters. Using the data of Fig. 11 to calculate NPQ as Fm/Fm′ – 1 (Stern–Volmer formulation), it can be shown that, when using $\Phi^A Fm'$ instead of $\Phi^E Fm'$, estimates of NPQ are prone to marked overestimation by more than 100% over

the lower range of irradiances and less at the higher range of irradiances (see Supporting Information Figs. S3 & S4).

Estimation of Fm′ by MPF's can also lead to a more robust assessment of parameters such as g_m that require estimates of J as input. The variable J method for estimating g_m can be strongly sensitive to the accuracy of J (Harley *et al*. 1992; Pons *et al*. 2009), and hence Fm′. In sunflower, differences in $\Phi^A Fm'$ and $\Phi^E Fm'$ (Fig. 11D) gave rise to pronounced differences in the corresponding values of J (Fig. 11F), especially at higher PPFD's; this lead to estimates of g_m based on $\Phi^A Fm'$-derived values of J that were highly erratic and essentially meaningless (Table 4). By contrast, mean g_m values calculated from $\Phi^E Fm'$-derived estimates of J (Table 4) were largely constant and showed uniform standard deviations across the same range of irradiances. Because all other input parameters were effectively equal, for example A_n, C_i, *etc*. (Table 4), these results suggest that the unrealistic g_m values we observed using $\Phi^A Fm'$-derived values of J were ultimately due to underestimation of true Fm′, which is a problem that can be largely avoided using the MPF approach and $\Phi^E Fm'$ to compute J.

The amplitude of the underestimation of Fm′ resulting from the use of a single SP as opposed to the MPF approach was dependent on plant growth conditions, where a larger effect was observed for plants grown in the field than for those grown in growth cabinets (Supporting Information Table S1). This could be due to the enhanced electron transport rate capacity of plants grown at high irradiance and/or temperature, issues that we have begun to investigate. Importantly, whereas the MPF approach provided improved estimates of Fm′ (i.e. in light-adapted states), it often failed to provide accurate estimate of Fm in leaves that had been dark-adapted for long periods (data not shown). In this condition, the duration of phase 1 of MPF that is optimal for the light adapted state is too short to reach steady state (data not shown) and the conventional single SP approach should be favoured.

The MPF method alleviates the need to use potentially problematic high intensity pulses

The saturation pulse method requires the assumptions that rate constants for processes other than PSII-mediated electron transfer (i.e. k_F, k_D, etc.) remain invariant during the pulse and that auxiliary reactions are not induced; however, there is potential for these assumptions to be violated when using intense Q′. Many different phenomena have been implicated in modulating SP-induced fluorescence yield (Kramer & Crofts 1996; Schreiber 2004). On the one hand, intense Q′ can induce auxiliary reactions, for example reaction centre quenching, formation of chlorophyll cations, and chlorophyll triplets, all of which can quench fluorescence. On the other hand, several auxiliary reactions are dependent upon the pH of the thylakoid lumen and are thus susceptible to turnover during the time of a saturating flash; the likelihood that such phenomena may occur increases with increasing intensity and duration of Q′. Any of these extraneous quenching phenomena may be manifested during an MPF as a lowering of the phase 3 ΦF relative to that attained during phase 1 (Fig. 3). While there were no significant differences between phases 1 and 3 ΦFs in sunflower (Fig. 10), phase 3 ΦFs in both maize and bean were observed to be progressively lower than those during phase 1 during a series of increasingly intense MPF's (data not shown). These results suggest that some of the types of extraneous quenching phenomena may have been progressively induced at higher pulse intensities. Moderate pulse intensities can minimize these auxiliary quenching phenomena, and yet they can nonetheless provide accurate estimates of Fm′ when combined with MPF dynamics (Fig. 10). Thus, the MPF method can be viewed as a dually beneficial approach because it provides accurate estimates of Fm′ while simultaneously avoiding high pulse intensities that can be problematic. The approach has been validated in leaf studies using land plants but is likely to also be important for improving chlorophyll fluorescence measurements in other photosynthetic taxa such as green algae. This is under current investigation.

ACKNOWLEDGMENTS

The authors wish to gratefully acknowledge Dr. Hugh Earl for his helpful insight during early stages of this work, Dr. Patrick Morgan for many useful discussions and for reading and improving the manuscript, and Mr. Robert Burns for his help in performing some of the field measurements.

AUTHOR CONTRIBUTIONS

S.L., T.A. & J.W. performed the experiments; R.E., B.R. & J.W. engineered and custom built the fluorometer and instrument software; B.G. authored the MPF principle, the simulation model and its software implementation; S.L., T.A., J.W., D.M. & B.G. contributed to the design and interpretation of the research and to the writing of the paper.

CONFLICT OF INTEREST

B.G. is member of the Science Advisory Board and a consultant for LI-COR Biosciences.

REFERENCES

Avenson T.J., Cruz J.A., Kanazawa A. & Kramer D.M. (2005) Regulating the proton budget of higher plant photosynthesis. *Proceedings of the National Academy of Sciences of the United States of America* **102,** 9709–9713.

Baake E. & Schloder J.P. (1992) Modeling the fast fluorescence rise of photosynthesis. *Bulletin of Mathematical Biology* **54,** 999–1021.

Bradbury M. & Baker N.R. (1981) Analysis of the slow phases of the in vivo chlorophyll fluorescence induction curve. Changes in the redox state of photosystem II electron acceptors and fluorescence emission from photosystems I and II. *Biochimica et Biophysica Acta* **635,** 542–551.

von Caemmerer S. (2000) *Biochemical Models of Leaf Photosynthesis*. Canberra, Australia: CSIRO Publishing.

Dietz K.J., Schreiber U. & Heber U. (1985) The relation between the redox state of Q_A and photosynthesis in leaves at various carbon dioxide, oxygen, and light regimes. *Planta* **166,** 219–226.

Earl H.J. & Ennahli S. (2004) Estimating photosynthetic electron transport via chlorophyll fluorometry without photosystem II light saturation. *Photosynthesis Research* **82,** 177–186.

Genty B., Briantais J.M. & Baker N.R. (1989) The relationship between the quantum yield of photosynthetic electron transport and photochemical quenching of chlorophyll fluorescence. *Biochimica et Biophysica Acta* **990,** 87–92.

Harbinson J. & Foyer C.H. (1991) Relationships between the efficiencies of photosystems I and II and stromal redox state in CO_2-free air. *Plant Physiology* **97,** 41–49.

Harley P.C., Loreto F., Di Marco G. & Sharkey T.D. (1992) Theoretical considerations when estimating the mesophyll conductance to CO_2 flux by analysis of the response of photosynthesis to CO_2. *Plant Physiology* **98,** 1429–1436.

Joliot P. & Joliot A. (1964) Etudes cinétique de la réaction photochimique libérant l'oxygène au cours de la photosynthèse. *Comptes Rendus de l'Académie des Sciences* **258,** 4622–4625.

van Kooten O. & Snel J.F.H. (1990) The use of chlorophyll fluorescence nomenclature in plant stress physiology. *Photosynthesis Research* **25,** 147–150.

Krall J.P. & Edwards G.E. (1990) Quantum yields of photosystem II electron transport and carbon dioxide fixation in C_4 plants. *Australian Journal of Plant Physiology* **17,** 579–588.

Krall J.P. & Edwards G.E. (1992) Relationship between photosystem-II activity and CO_2 fixation in leaves. *Physiologia Plantarum* **86,** 180–187.

Kramer D.M. & Crofts A.R. (1996) Control and measurement of photosynthetic electron transport *in vivo*. In *Photosynthesis and the Environment* (ed. N.R. Baker), pp. 25–66. Kluwer Academic Publishers, Dordrecht, The Netherlands.

Kroon B.M.A. & Thoms S. (2006) From electron to biomass: a mechanistic model to describe phytoplankton photosynthesis and steady-state growth rates. *Journal of Phycology* **42,** 593–609.

Laisk A. & Loreto F. (1996) Determining photosynthetic parameters from leaf CO_2 exchange and chlorophyll fluorescence. *Plant Physiology* **110,** 903–912.

Lavergne J. & Trissl H.-W. (1995) Theory of fluorescence induction in photosystem II: derivation of analytical expressions in a model including exciton-radical-pair equilibrium and restricted energy transfer between photosynthetic units. *Biophysical Journal* **68,** 2474–2492.

Lazar D. (2003) Chlorophyll *a* fluorescence rise induced by high light illumination of dark-adapted plant tissue studied by means of a model of photosystem II and considering photosystem II heterogeneity. *Journal of Theoretic Biology* **220,** 469–503.

Loriaux S.D., Burns R.A., Welles J.M., McDermitt D.K. & Genty B.E. (2006) Determination of maximal chlorophyll fluorescence using a multiphase single flash of sub-saturating intensity. *American Society of Plant Biologists Annual Meeting*, Boston, M.A., poster P13011 (http://abstracts.aspb.org/pb2006/public/P13/P13011.html).

Markgraf T. & Berry J. (1990) Measurement of photochemical and non-photochemical quenching: correction for turnover of PS2 during steady-state photosynthesis. In *Current Research in Photosynthesis* (ed. M. Baltscheffsky), pp. 279–282. Kluwer Academic Publishers, Dordrecht, the Netherlands.

Ogren E. & Baker N.R. (1985) Evaluation of a technique for the measurement of chlorophyll fluorescence from leaves exposed to continuous white light. *Plant, Cell and Environment* **8,** 539–547.

Pons T.L., Flexas H., von Caemmerer S., Evans J.R., Genty B.E., Ribas-Carbo M. & Brugnoli E. (2009) Estimating mesophyll conductance to CO_2: methodology, potential errors, and recommendations. *Journal of Experimental Botany* **60,** 2217–2234.

Renger G. & Schulze A. (1985) Quantitative analysis of fluorescence induction curves in isolated spinach chloroplasts. *Photobiochemistry and Photobiophysics* **9,** 79–87.

Ruuska S.A., Badger M.R., Andrews T.J. & von Caemmerer S. (2000) Photosynthetic electron sinks in transgenic tobacco with reduced amounts of Rubisco: little evidence for significant Mehler reaction. *Journal of Experimental Botany* **51,** 357–368.

Schreiber U. (2004) Pulse-amplitude-modulation fluorometry and saturation pulse method: an overview. In *Advances in Photosynthesis and Respiration* (eds G.C. Papageorgiou & Govindjee), pp. 279–319. Springer, Dordrecht, the Netherlands.

Schreiber U., Schliwa U. & Bilger W. (1986) Continuous recording of photochemical and non-photochemical chlorophyll fluorescence quenching with a new type of modulation fluorometer. *Photosynthesis Research* **10,** 51–62.

Stirbet A., Govindjee, Strasser B.J. & Strasser R. (1998) Chlorophyll a fluorescence induction in higher plants: modelling and numerical simulation. *Journal of Theoretical Biology* **193,** 131–151.

Vrabl D., Vaskova M., Hronkova M., Flexas J. & Santrucek J. (2009) Mesophyll conductance to CO(2) transport estimated by two independent methods: effect of variable CO(2) concentration and abscisic acid. *Journal of Experimental Botany* **60,** 2315–2323.

Zhu X.-G., Govindjee, Baker N.R., deStruler E., Ort D.R. & Long S.P. (2005) Chlorophyll *a* fluorescence induction kinetics in leaves predicted from a model describing each discrete step of excitation energy and electron transfer associated with photosystem II. *Planta* **223,** 114–133.

Received 20 December 2012; received in revised form 27 March 2013; accepted for publication 28 March 2013

SUPPORTING INFORMATION

Additional Supporting Information may be found in the online version of this article at the publisher's web-site:

Figure S1. Simulated effect of Q′ on $\Phi^A Fm'$ and $\Phi^E Fm'$. Simulated estimates of $\Phi^A Fm'$ (closed symbols) were computed using a range of steady irradiances between 5000–15 000 μmol photons $m^{-2}\,s^{-1}$. Three different electron transport and qN capacities were used during simulations by varying k_{ox} and k_D, respectively, according to: $k_{ox} = 50\ s^{-1}$; $k_D = 0.244 * 10^9\ s^{-1}$ (black squares); $k_{ox} = 50\ s^{-1}$; $k_D = 5 * 10^9\ s^{-1}$ (red circles); and $k_{ox} = 200\ s^{-1}$; $k_D = 5 * 10^9\ s^{-1}$ (blue triangles). The corresponding estimates of $\Phi^E Fm'$ (open symbols) were obtained by ramping the steady irradiances by 25% at a rate of 0.01 mol photons $m^{-2}\,s^{-2}$ and performing linear regression of the resultant ΦF plotted against $(Q')^{-1}$ and extrapolation to the *y*-intercept. All values of $\Phi^A Fm'$ and $\Phi^E Fm'$ are normalized to the corresponding ΦF at infinite irradiance.

Figure S2. Simulated effect of Q′ on the variable part of $\Phi^A Fm'$ and Q_A^- (i.e. 1-q). The variable part of $\Phi^A Fm'$ was calculated as $\Phi^A Fv' = \Phi^A Fm' - \Phi Fo'$. Simulated estimates of $\Phi^A Fv'$ (A) and (1-q) (B) were computed using a range of steady irradiances between 5000–15000 μmol photons $m^{-2}\,s^{-1}$. Three different electron transport and qN capacities were used during simulations by varying k_{ox} and k_D, respectively, according to: $k_{ox} = 50\ s^{-1}$; $k_D = 0.244 * 10^9\ s^{-1}$ (black squares); $k_{ox} = 50\ s^{-1}$; $k_D = 5 * 10^9\ s^{-1}$ (red circles); and $k_{ox} = 200\ s^{-1}$; $k_D = 5 * 10^9\ s^{-1}$ (blue triangles). All values of $\Phi^A Fv'$ are normalized to the $\Phi Fv'$ at infinite irradiance.

Figure S3. Experimental effect of MPF protocol on estimation of NPQ. Leaves of maize (A) and sunflower (B) were exposed to a range of PPFD, as described in the legend of Fig. 11. Estimates of NPQ were calculated as $\Phi Fm/\Phi Fm' - 1$ using RF-derived values of $\Phi^A Fm'$ (black squares) or MPF-derived values of $\Phi^E Fm'$ (red circles) (see legend of Fig. 11). Values of ΦFm used for calculation of NPQ were obtained 5 minutes after cessation of actinic illumination at the lowest PPFD. Each maize data point is the mean of 9 to 14 observations (± SD), and each sunflower data point is the mean of 7 to 9 observations (± SD). Paired comparisons of the mean NPQ between the MPF and RF methods were significant ($p < 0.01$) at all PPFD.

Figure S4. Relative effect of MPF protocol on fluorescence parameters. Estimates of Fm′ (black squares), Φ_{PSII} (red circles), and NPQ (blue triangles) were obtained using RF

and MPF methodologies, as described in legends of Fig. 11 and S3. The relative effect of the MPF-derived values on estimation of these fluorescence parameters in maize (A) and sunflower (B) were obtained as the ratio of the respective MPF-derived and RF-derived parameter.

Table S1. Effect of MPF on Fm′ and Φ_{PSII} in various species and growth conditions. Using a range of species grown under various conditions, Fm′ was estimated using RFs and MPFs whose maximum intensities were ~7000 μmol m^{-2} s^{-1}. Mean percent effects on Fm′ are expressed as: $(\Phi^{E}Fm'/\Phi^{A}Fm' - 1) * 100$. The effects on corresponding values of Φ_{PSII} are also shown. $^{M}T_{leaf}$ and ^{M}PPFD are leaf temperature and PPFD, respectively, during measurements. All values represent means ± SD for reported n-plants.